Environmental and Earth Sciences Research Journal
Vol. 12, No. 4, December, 2025, pp. 32-38
Journal homepage: http://iieta.org/journals/eesrj

Petrography Analysis and Influence of Density on the Electrical Resistivity of Geological Formations: Case Study of a Locality in Batié, West Cameroon

Kenfack Jean Victor[1*], Tchomtchoua Tagne Stéphane[1], Njanko Théophile[1,2], Teikeu Ngueveu Eric Donald[1]

[1] Laboratory of Environmental Geology, Department of Earth Sciences, University of Dschang, Dschang P.O. Box 67, Cameroon
[2] Ministry of Scientific Research and Innovation, DPSP/CCAR, Yaoundé P.O. Box 1457, Cameroon

Corresponding Author Email: victor.kenfack@univ-dschang.org

Copyright: ©2025 The authors. This article is published by IIETA and is licensed under the CC BY 4.0 license (http://creativecommons.org/licenses/by/4.0/).

https://doi.org/10.18280/eesrj.120401

Received: 6 August 2025
Revised: 27 November 2025
Accepted: 5 December 2025
Available online: 31 December 2025

Keywords:
petrography, electrical resistivity, density, reflection coefficient, Batié

ABSTRACT

This study was conducted in the Bahiala village in the West region of Cameroon. The aim of this study is to show how the petrography type and density of formations influence the resistivity of geological formations using Vertical Electrical Soundings (VES) and laboratory analyses. Petrographic analysis was performed on two rock samples. Forty-five VES were conducted, revealing resistivities ranging from 53.86 Ω·m to 39,890 Ω·m. Density measurements were carried out on fifteen rock samples, yielding values between 2.09 and 3. The petrographic analysis shows that the area is covered by biotite granites and trachytes with calcite geodes. The 1D inversion of the apparent resistivities shows surface layers consisting in places of sandy-clayey materials and more or less silty laterites. The densities of the outcropping geological formations vary between 2.090 g/cm^3 and 3.000 g/cm^3. The low electrical resistivity domain corresponds to the high-density domain and the domains where the geological formations are less fractured due to the high reflection coefficient values observed. The higher densities of the geological formations indicate the less aquifers presence.

1. INTRODUCTION

The materials of the earth's crust are characterized by their chemical, physical and mechanical properties, all of which are interrelated. The mineralogy of a rock, conditioned by its chemical composition, has a significant influence on its physical properties such as magnetic susceptibility, density, conductivity and electrical resistivity. All these properties are influenced by the chemical composition of the rocks. This is due to the molar mass of the chemical elements, which essentially constitute the minerals of the rocks, and the ability of each ion to carry the electric current. These properties vary for the same original material depending on factors such as climate and topography among others.

Electrical resistivity refers to a material's inherent capacity to resist the flow of electric current. In geophysical investigations, this property often exhibits significant variations, making it a key parameter for subsurface characterization. Resistivity is largely influenced by the ionic composition and especially by the water content of the medium, which governs its electrolytic conductivity. Minor variations in resistivity may also result from changes in surface topography. According to Obiora et al. [1] and Choudhury et al. [2], in a uniform geological medium, resistivity values tend to drop by approximately 20 to 40% when measurements are taken at elevated positions (such as hilltops), and increase by about 20 to 50% in low-lying areas such as valley bottoms.

The density of a material is defined as the ratio between its mass per unit volume and that of water. It is determined primarily by the chemical and mineralogical makeup of the material. Most rocks in the Earth's crust are composed mainly of eight major elements: oxygen (46.5%), silicon (28%), aluminum (8%), iron (5%), calcium (3.5%), sodium (3%), potassium (2.5%), and magnesium (2%), alongside trace elements and rare earths.

By combining electrical resistivity measurements at various depths with density data from surface geological formations, it becomes possible to identify spatial trends and correlations. These variations often reflect the underlying petrographic characteristics of the formations.

While prior geological [1, 3, 4], hydrogeological investigations [5] and hydrogeophysical investigations [6] have been conducted in the Batié region, the influence of surface rock density on surface electrical resistivity remains unexplored, which motivates the present study.

2. STUDY AREA

The study site is geographically positioned between longitudes 10°18'55" and 10°17'00" East, and latitudes 5°18'25" and 5°16'20" North, with elevations ranging from 1560 to 1720 meters above sea level. It is located in the village of Bahiala, within the Batié Subdivision in the western region of Cameroon, encompassing a perimeter of approximately 12.7 kilometers and covering a surface area of around 9.1

square kilometers (Figure 1).

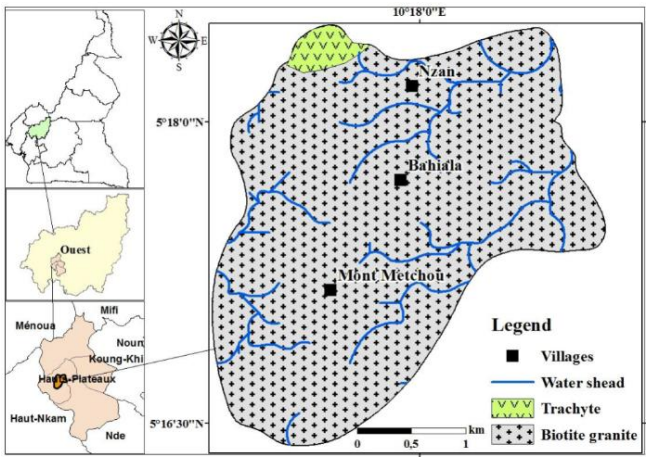

Figure 1. Location and geological map
Modified from a previous study [4]

From a climatic perspective, the region experiences a temperate tropical climate. Rainfall patterns show significant seasonal variation, with monthly averages ranging from 11 mm in December to a peak of 328 mm in September, culminating in an annual average of about 1894 mm. Temperature fluctuations are moderate, with monthly averages spanning from 17.6°C in July to 20.3°C in March, yielding an annual mean temperature close to 19°C and a thermal amplitude of roughly 2.7°C.

Topographically, the area features diverse reliefs, including rolling hills, steep slopes, and undulating terrain. Elevations across the landscape vary, reaching up to 1720 meters at Mount Metchou.

3. GEOLOGICAL SETTING

From a geological standpoint, the study area lies along the Central African Panafrican Belt (CAPB), a megastructure dated between 650 and 540 Ma. The study area rests on a granito-gneissic basement. The area is characterized by a syn-tectonic granite body, aligned with the axis of the major Batié anticlinorium, as described by Mihret and Wuletaw [7] and Jimoh et al. [8]. Some isolated trachytic intrusions have also been identified in the region [9].

Petrographic observations reveal that the granite displays a monzonitic texture with an alkaline affinity. It is distinguished by large, reddish-pink phenocrysts, often described as resembling "horse teeth" that may reach sizes of 7–8 cm in length and 4–5 cm in width [7]. The groundmass is a medium grayish matrix enriched in biotite and alkali plagioclase [9]. These granitic bodies appear as prominent, rounded hills across the Batié and Baham areas, as well as the highlands of Mifi.

Geochemical data, which align closely with those obtained from the Dschang granite, indicate a composition dominated by 70–75% SiO_2, 11–15% Al_2O_3, 2–3% Fe_2O_3, and between 0–1.5% MnO and MgO, along with 3.5–5.5% combined Na_2O and K_2O contents [2, 4, 7, 9].

4. METHODOLOGY

This work is based on petrographic analysis, Vertical Electrical Soundings (VES) and density measurements.

The petrographic analysis consists of sampling the different petrographic types observed in the study area, to make their macroscopic and microscopic descriptions. Rock samples are prepared as thin sections and then analyzed petrographically using a polarizing microscope. This analysis identifies the mineralogical composition based on texture, optical properties, alteration, and mineral relationships, enabling the naming and classification of the rocks by their petrographic type.

VES were conducted using a 4Point light resistivimeter to determine the vertical distribution of apparent resistivities. This method involves injecting a direct current into the ground through a pair of current electrodes and measuring the resulting potential difference across a second pair of potential electrodes. The survey was performed using the Schlumberger array configuration.

As illustrated in Figure 2, the technique consists of injecting a direct current (I) into the subsurface using two outer electrodes (A and B), while the potential difference (ΔV) is recorded between two inner electrodes (M and N). During the survey, the spacing between the current electrodes is gradually increased to investigate deeper layers, and the spacing of the potential electrodes is also adjusted accordingly to maintain measurement sensitivity [7, 9, 10-14].

$$\rho = k\frac{\Delta V}{I}, \text{ where } k = \pi\frac{(\frac{AB}{2})^2-(\frac{NM}{2})^2}{NM} \quad (1)$$

where,
ΔV = measured potential difference;
I = injected current intensity.

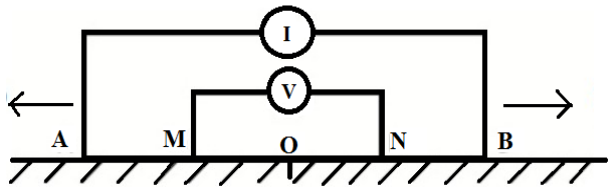

Figure 2. Schlumberger quadruple device

The rock samples taken from the various outcrops in slab or ball rock were weighed using a sensitive electronic balance and quantified using a volumetric device. The mass and volume of the samples made it possible to obtain the specific density by the ratio mass to volume (2) (g/ml); then the different densities were obtained by dividing the specific density of each sample by the density of water (3).

$$\rho_s = \frac{m}{V} \quad (2)$$

$$d = \frac{\rho_s}{\rho_w} \quad (3)$$

where, m: the mass of the sample; V : the volume of the sample; ρ_w : the density of water, and d: the density. Rock samples are taken from the outcrops along with their coordinates, and then these samples are cut to have measurable volumes (Figure 3(a) and 3(b)). Subsequently, using a volumetric device and a sensitive balance (Figure 3(c)), the volume (ml) and mass (g) are measured, respectively. This

measurement was carried out in fifteen stations distributed over the sampling map, as shown in Figure 3.

Figure 3. Rock density measurement. a) Granite samples; b) Volcanic rock sample; c) Measuring operation

A total of 45 VES points were acquired and spatially distributed as indicated on the sampling map (Figure 4). The apparent resistivity values recorded at an electrode spacing of AB/2 = 1.5 m were used to construct an isoresistivity contour map, following approaches similar to those described by Stephane et al. [6] and Choudhury et al. [2].

The dataset was subjected to 1D inversion using the Jointem software, enabling the estimation of true resistivity values and corresponding layer thicknesses. Interpretation of the resulting 1D resistivity models facilitates the delineation of potential aquifer horizons and their electrical characteristics.

These resistivity values were subsequently used to compute the reflection coefficient (1), a parameter indicative of the degree of fracturing or porosity contrast between geological layers, particularly between the aquifer and the overlying formation, as proposed by Oladunjoye et al. [14].

$$R_c = \frac{\rho_n - \rho_{(n-1)}}{\rho_n + \rho_{(n-1)}} \quad (4)$$

where, ρ_n is the resistivity of the aquifer layer and $\rho_{(n-1)}$ is the resistivity of the layer directly above the aquifer.

The sampling map (Figure 4) covers a perimeter of about 12.7 km, an area of about 9.1 km², and has forty-five VES stations, fifteen density points and two rock sampling points.

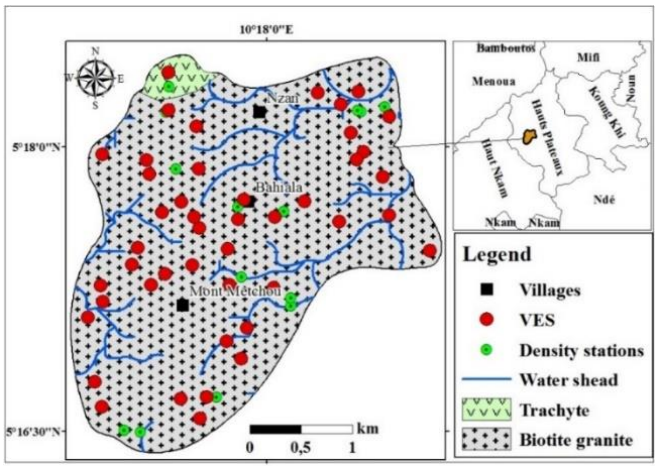

Figure 4. Sampling map

Maps of apparent isoresistivity (AB/2 = 1.5), density, and reflection coefficient were produced by ordinary kriging with the ArcGIS 10.4 software.

5. RESULTS AND DISCUSSIONS

5.1 Petrographic analyses

Petrographic analysis of the plutonic formations (Figure 5(a) and 5(b)) reveals a mineral assemblage that includes biotite (Figures 5(e) and 5(g)), green hornblende (Figure 5(g)), plagioclase (Figure 5(d)), quartz (Figures 5(d) and 5(h)), potassium feldspath (Figures 5(d), 5(g), and 5(h)), sphene (Figure 5(e)), apatite, and opaque minerals (Figures 5(e) and 5(g)). These rocks correspond to biotite-rich granites with a porphyroid and granular texture. Such characteristics are consistent with earlier findings [4, 7-9].

Field investigations also identified volcanic rocks in the northern part of the study area, particularly near Nzan (Figure 5(c)), a feature not documented on the existing geological maps adapted from a previous study [3]. These volcanic outcrops were observed at coordinates E 10°17'29" / N 5°18'19.7" at an elevation of 1636 meters, and E 10°17'31.6" / N 5°18'23.6" at 1626 meters. The rocks are characterized by the presence of geodes, a diagnostic feature previously reported by Ibagbo et al. [15] in volcanic terrains of western Cameroon.

Microscopic examination of the volcanic rock samples indicates a sub-trachytic texture and the presence of key mineral phases, including plagioclase (Figures 5(f) and 5(i)), sanidine microlites (Figure 5(f)), opaque minerals, and a vitreous groundmass.

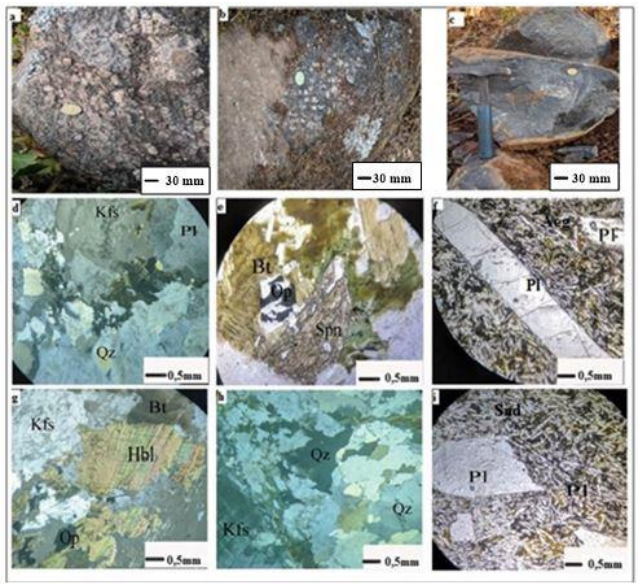

Figure 5. Geological formations of the study area. a) Granite outcrop; b) Granite boulder; c) Block of volcanic rock; d) Zone of k-feldspath, quartz and plagioclase; e) Zone of Biotite and sphene; f) Zone of k-feldspath, plagioclase and opaque minerals; g) Zone of opaque minerals, hornblende, biotite, and k-feldspar; h) Zone of quartz and k-feldspar; i) Zone of plagioclase and sanidine

5.2 Geoelectrics analysis

The interpretation of VES data led to the classification of the results into seven distinct geoelectrical anomaly types: H, K, Q, HK, KH, HKH, and KHK. These types exhibit apparent resistivity values ranging from 53.86 Ω·m to 39.890 Ω·m. The anomalies were examined in light of petrographic

characteristics, weathering profiles, and topographic positions (e.g., hilltops, mid-slopes, and valley bottoms), following a similar interpretative approach to that used by these studies [1, 6, 13-15].

- Type H is characterized by a relatively resistive upper layer of sandy-clay, underlain by a conductive horizon associated with fractured material, typically forming a concave (boat-shaped) profile above a moderately resistive basement (Figure 6(a)).
- Type K shows a resistive gravel-rich intermediate layer between two conductive horizons: a topsoil layer of sandy loam and a deeper sandy-clay unit overlying a moderately fractured substratum (Figure 6(b)).
- Type Q displays a surface lateritic layer, followed by a clayey-sandy horizon and a fractured basement. It usually represents a downward transition from resistive to more conductive zones (Figure 6(c)).

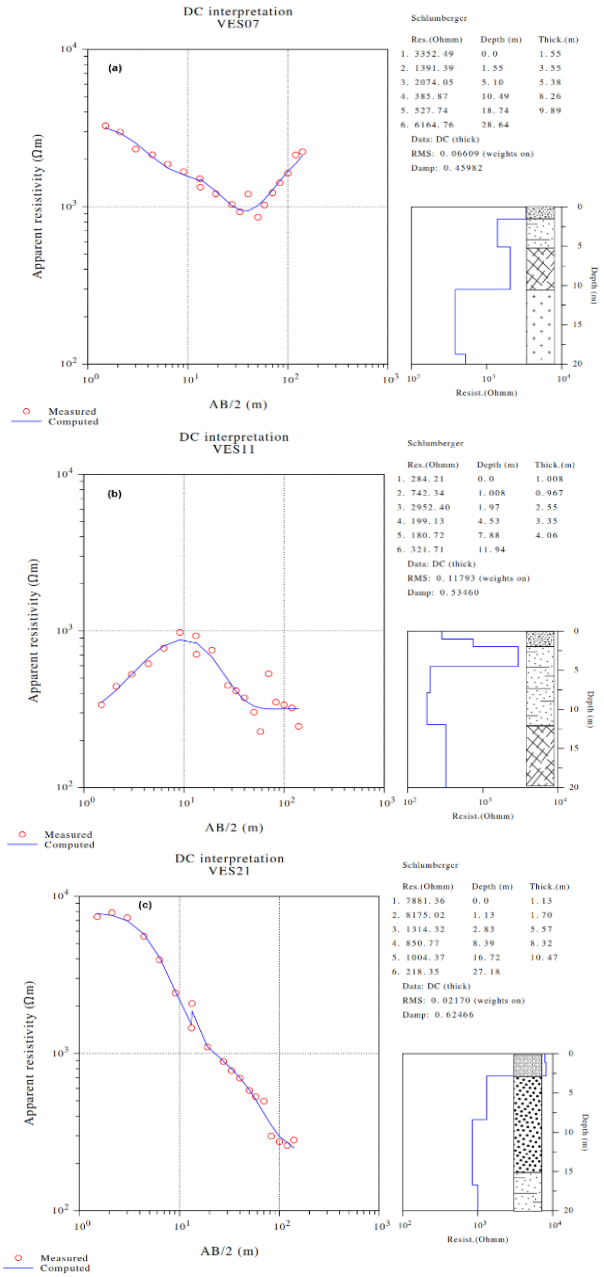

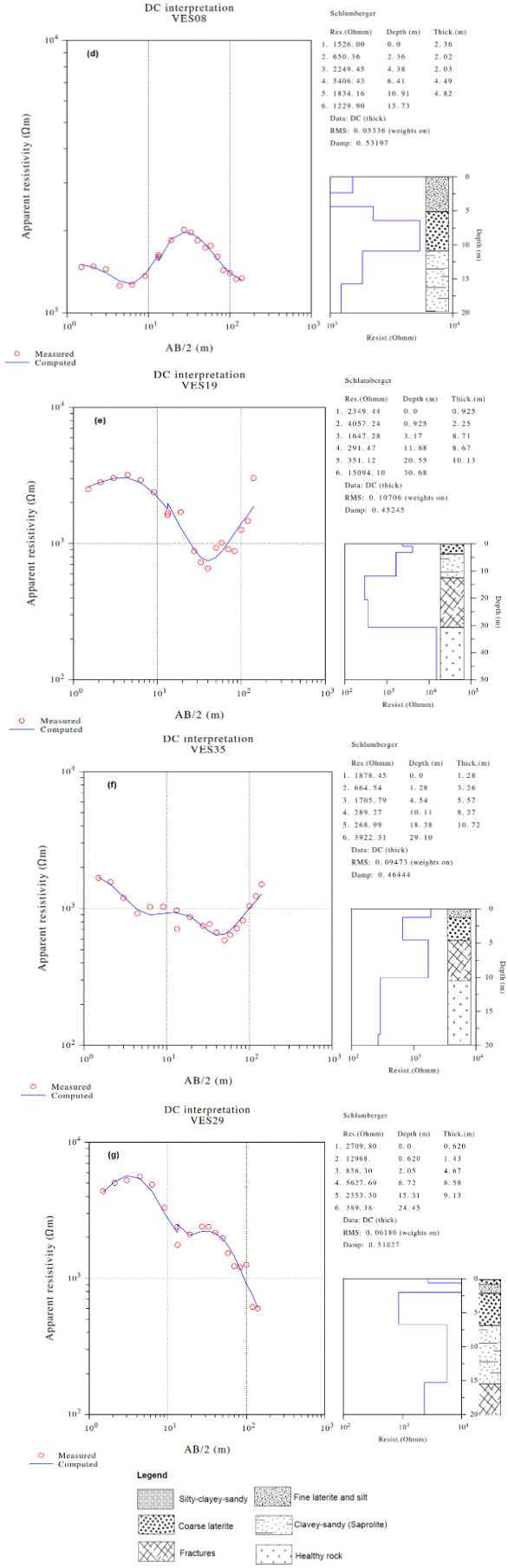

Figure 6. VES curves. a) Type H curve; b) Type K curve; c) Type Q curve; d) Type HK curve; e) Type KH curve; f) Type HKH curve; g) Type KHK curve

- Type HK consists of a moderately conductive topsoil, an intermediate conductive gravel zone, and a deeper conductive clay-sand unit that often reaches the weathered bedrock (Figure 6(d)).
- Type KH features a central gravelly resistive layer flanked by conductive horizons, indicating weathered and saturated materials at depth (Figure 6(e)).
- Type HKH presents a gravel-rich resistive layer sandwiched between a conductive silt-sand surface layer and a deeper conductive clay-sand horizon above a semi-weathered base (Figure 6(f)).
- Type KHK begins with a weakly conductive topsoil, followed by conductive gravel and clay-sand layers, underlain by a fractured and increasingly resistive basement (Figure 6(g)).

The variability observed among these curve types is primarily attributed to the heterogeneous nature of surficial and subsurface materials, as well as the degree of moisture content. These materials range from coarse laterites to cultivable silty and clayey-sandy soils, consistent with the findings of these studies [6, 14], which noted the structural complexity of surface layers in VES interpretations. Additionally, the morphological setting marked by steep, sloping, and undulating terrains further influences curve geometry, as highlighted by Oladunjoye et al. [14].

In general, the H, KH, and HKH types are associated with surface clayey-sandy horizons and granite outcrops (balls or slabs) that show limited weathering. In contrast, the HK, K, and Q types often correspond to incomplete borehole penetration profiles, where resistivity signatures indicative of fresh bedrock are absent. These anomalies suggest thicker weathered mantles and the absence of competent surface outcrops, consistent with the presence of coarse laterites and highly fractured deeper zones [9].

5.3 Rocks density

The measured density values of the rock samples range from 2.090 to 3.000 g/cm³, based on 4 to 6 samples collected from each outcrop, following the protocol described in the methodology section. These values are summarized in Table 1.

Table 1. Densities values

Stations	Average Densities (g/cm³)	Observations
D1	2.520	Weathered granite
D2	2.090	Weathered granite
D3	2.200	Weathered granite
D4	2.270	Weathered granite
D5	2.580	Weathered granite
D6	2.570	Weathered granite
D7	2.440	Weathered granite
D8	2.600	Weathered granite
D9	2.570	Weathered granite
D10	2.420	Weathered granite
D11	2.310	Weathered granite
D12	2.310	Weathered granite
D13	2.550	Weathered granite
D14	2.530	Weathered granite
D15	3.000	Healthy trachyte

The spatial distribution of both surface resistivity values (measured at AB/2 = 1.5 m) and density data reveals notable correlations across specific zones of the study area, particularly in regions labeled A, B, C, D, and E (Figures 7(a) and 7(b)). Areas A and B demonstrate that zones with higher rock densities tend to exhibit lower surface resistivities, suggesting the presence of compact, unweathered rock with limited alteration. In contrast, zone D exhibits the opposite trend, where lower densities correspond to elevated resistivity values. Zones C and E display intermediate characteristics, with moderate values for both parameters.

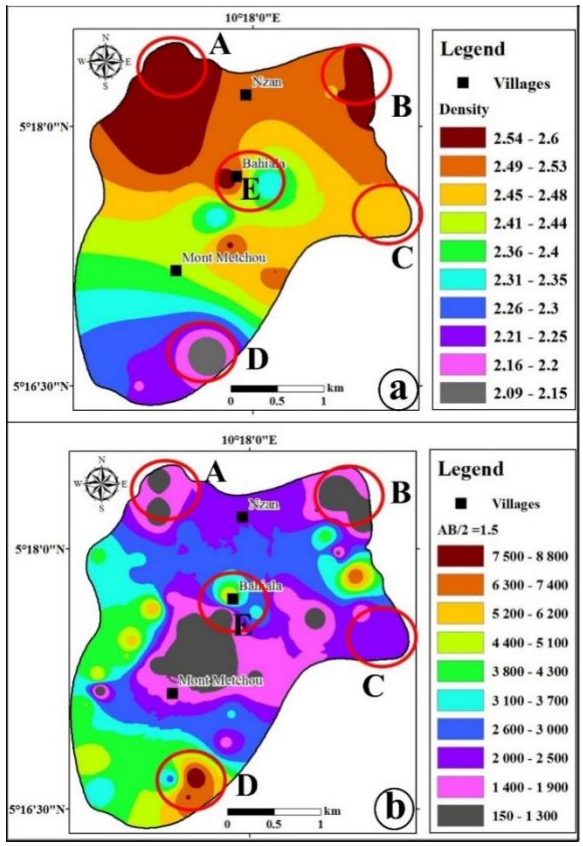

Figure 7. Spatial variations of the parameters: a) Densities; b) Isoresistivity at AB/2 = 1.5 m

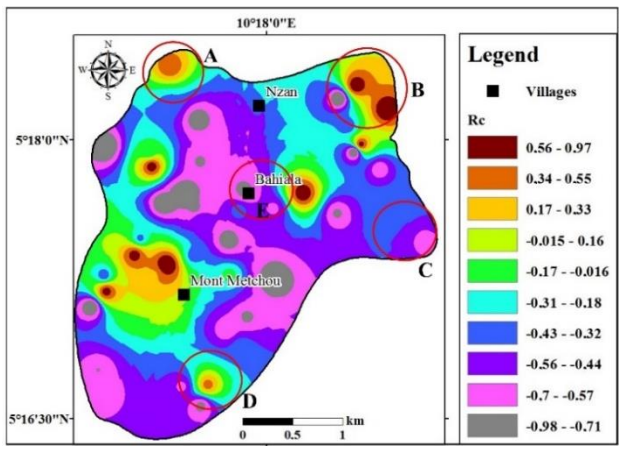

Figure 8. Spatial variation of reflexion coefficient

Zones characterized by high densities and low surface resistivities are associated with visible rock outcrops and a lack of lateritic cover, indicating that weathering processes have not significantly altered the bedrock, which retains much of its original geochemical composition.

Using the resistivity values associated with potential aquifer zones at each VES station, the reflection coefficient (Rc) was

calculated. The Rc values in the study area range from -0.977 to 0.966. The highest Rc values (from 0.966 to -0.184) are concentrated in the northeastern and southwestern regions, while lower Rc values are mainly observed in the central, southeastern, and southern parts of the study area (Figure 8).

In this context, higher Rc values indicate less fractured bedrock, while lower Rc values reflect more intensely fractured geological media. These observations align partially with those of Oladunjoye et al. [14], who reported Rc values ranging between -0.7514 and 0.9200 in southeastern Nigeria, and Obiora et al. [1], who found Rc values between 0.4 and 0.8 in crystalline rocks such as granite, quartzite, gneiss, and migmatitic gneiss in Oyo State, southwestern Nigeria. The latter authors considered Rc values below 0.4 as indicative of highly fractured aquifers. Additionally, aquifers with thicknesses exceeding 25 m and Rc values below 0.75 are considered hydrogeologically favorable.

The degree of fracturing, which directly affects the storage capacity of hard rock aquifers, plays a central role in groundwater potential. As previously emphasized by Jimoh et al. [8], rocks with low porosity and minimal fracturing are referred to as “dry rocks”, due to their limited capacity to retain water.

Regions A, B, and D (see Figure 8) correspond to zones with low aquifer fracturing potential. Areas A and B are characterized by high-density materials and low surface resistivity, while zone D shows the inverse pattern. The presence of lateritic soils in zone D points to advanced weathering, resulting in the leaching of alkali elements (and in some cases, silica) and the concentration of residual iron and aluminum, forming lateritic profiles. The loss of specific chemical constituents during weathering leads to a decrease in rock compactness, thereby reducing its bulk density.

The interpretation of geophysical data reveals distinct hydrogeological settings. Zones A and B, featuring relatively unaltered surface rocks (trachyte and granite) with high Rc and densities, indicate a shallow aquifer with rapid infiltration, possibly linked to sandy-clay lithologies. Zones C and E, moderately weathered and partially saturated, act as reservoirs and storage areas for porous aquifers, characterized by slow and gradual infiltration. Although distinct, zones A, B, and C contribute to aquifer recharge. Finally, zone D, located on lateritic soils (low density, high resistivity), potentially feeds deeper aquifers. These parameters, along with the aquifer types allows the characterisation of the fracture aquifers, porous aquifers and recharge zones.

6. CONCLUSION

Petrographic analyses indicate that the study area is predominantly composed of two main lithologies: biotite granite and trachyte, with biotite granite being the most spatially widespread. The interpretation of the inverted geoelectrical data reveals a variety of curve types, namely H, K, Q, HK, KH, HKH, and KHK, each associated with distinct geological structures that align well with field-based observations.

The measured rock densities range from 2.090 to 2.600 g/cm³, with higher density values primarily concentrated in zones A and B, while lower densities are more prevalent in zone D of the same figure.

The Rc distribution highlights that aquifers in zones A, B, and D exhibit lower levels of fracturing, which implies more compact geological formations in these regions. When analyzing the spatial patterns of surface resistivity, rock density, and reflection coefficient, a strong correlation emerges: areas with higher rock densities tend to have lower resistivity values near the surface, and vice versa. This relationship is particularly evident in zones A, B, C, D, and E.

These surface observations are significant because they reflect subsurface fracturing trends. Specifically, zones A and B, which show elevated surface densities and reduced surface resistivities, are also associated with less fractured aquifer systems at depth, as inferred from the Rc values. This suggests that denser surface rocks are indicative of less altered and more cohesive subsurface materials, with lower permeability due to limited fracturing. For future work in this area, the application of supplementary geophysical techniques seismic surveying, for instance, would likely lead to a more constrained understanding of subsurface structure and the nature of aquifer properties.

REFERENCES

[1] Obiora, D.N., Ibuot, J.C., Alhassan, U.D., Okeke, F.N. (2018). Study of aquifer characteristics in northern Paiko, Niger State, Nigeria, using geoelectric resistivity method. International Journal of Environmental Science and Technology, 15(11): 2423-2432. https://doi.org/10.1007/s13762-017-1612-8

[2] Choudhury, J., Kumar, K.L., Nagaiah, E., Sonkamble, S., Ahmed, S., Kumar, V. (2017). Vertical electrical sounding to delineate the potential aquifer zones for drinking water in Niamey city, Niger, Africa. Journal of Earth System Science, 126(6): 91. https://doi.org/10.1007/s12040-017-0860-9

[3] Kwékam, M., Talla, V. Fozing E.M., Tcheumenak Kouémo, J., Dunkl, I., Njonfang, E. (2020). The Pan-Africain high-K I-type granite from batié complex, West Cameroon: Age, origin, and tectonic implications. Frontiers in Earth Science, 8: 363. https://doi.org/10.3389/feart.2020.00363

[4] Wouatong, A.S.L., Yerima, B.P.K., Yongue Fouateu, R., Mvondo Ze, A., Ekodeck G.E. (2013). The origin of etch pits recorded on residual grain surfaces from kaolinized granitic rocks west region, Cameroon. Earth Science Research, 2(2): 93-110. https://doi.org/10.5539/esr.v2n2p93

[5] Mono, J.A., Bouba, A., Ngoh, J.D., Owono Amougou, O.U.I., Enyegue Nyam, F.M., Ndougsa Mbarga, T. (2024). Lineament mapping in Batie Area (West-Cameroon) using Landsat-9 operational land imager/thermal infrared sensor and shuttle radar topography mission data: Hydrogeological implication. Revue internationale de Géomatique, 33: 135-154. https://doi.org/10.32604/rig.2024.049966

[6] Stephane, T.T., Victor, K.J., Théophile, N., Donald, T.N.E., Rodrigue, T.T. (2024). Contribution of vertical electric sounding, Landsat 8 and SRTM images to hydrogeological characterization: Case study of Batié, West-Cameroon. Arabian Journal of Geosciences, 17(6): 173. https://doi.org/10.1007/s12517-024-11967-8

[7] Mihret, B., Wuletaw, A. (2025). The impact of geological structures on groundwater potential assessment in volcanic rocks in the Borena Sayint district, northwestern Ethiopian Plateau: A review.

Hydrology and Earth System Sciences, 29(13): 2951-2959. https://doi.org/10.5194/hess-29-2951-2025

[8] Jimoh, M.O., Opawale, G.T., Ejepu, J.S., Abdullahi, S., Agbasi, O.E. (2023). Investigation of groundwater potential using geological, hydrogeological and geophysical methods in Federal University of Technology, Minna, Bosso Campus, North Central, Nigeria. HydroResearch, 6: 255-268. https://doi.org/10.1016/j.hydres.2023.09.002

[9] Jude, N.N., Wotany, E.R., Agyingi, C., Nelson, M.A. (2024). Geological influence on groundwater quality in volcanic aquifers of Eastern Mount Cameroon, West of the Penda Mboko River. Discover Applied Sciences, 6: 541. https://doi.org/10.1007/s42452-024-06169-6

[10] Ajayi, T., Awotuyi, B., Bello, R. (2019). Geoelectric assessment of groundwater potential in Supare Akoko, Southwestern, Nigeria. Environmental & Earth Sciences Research Journal, 6(2): 59-70. https://doi.org/10.18280/eesrj.060202

[11] Kouakou, K.E.G., Kouadio, K.E., Keita, D., Kouame, L.N., Sombo, A.P. (2017). Groundwater exploration in the Niellé region (Northern Ivory Coast): Efficiency of the electrical resistivity method. European Scientific Journal, 13(6): 206. https://doi.org/10.19044/esj.2017.v13n6p206

[12] Abasoh, M.E., Victor, K.J., Pierre, W., Anoh, N.O., Jude, P.N., Roosvelt, D.M.M., Tabod, T.C. (2022). Hydrogeological mapping from Landsat 8, SRTM images, vertical electrical soundings and hydraulic parameters of aquifers: Case study of the South Western part of Baleng Watershed. Results in Geophysical Sciences, 9: 100040. https://doi.org/10.1016/j.ringps.2022.100040

[13] Jude, P.N., Victor, K.J., Pierre, W., Anoh, N.O., Abasoh, M.E., Rosvelt, D.M.M., Tabod, T.C. (2021). Petrographic, morpho-structural and geophysical study of the quartzite deposit in the central part of Pouma, Littoral-Cameroon. Geophysical Sciences, Results in Geophysical Sciences, 7: 100019. https://doi.org/10.1016/j.ringps.2021.100019

[14] Oladunjoye, M.A., Adefehinti, A., Ganiyu, K.A.O. (2019). Geophysical appraisal of groundwater potential in the crystalline rock of Kishi area. Journal of African Earth Sciences, 151: 107-120. https://doi.org/10.1016/j.jafrearsci.2018.11.017

[15] Ibagbo, A.A., Omosuyi, G.O., Ojo, T.B., Abiola, A. (2017). Groundwater potential evaluation in a typical basement complex environment using GRT Index–A case study of Ipnsia-Okeodu area near Akure, Nigeria. Journal of Geoscience and Environment Protection, 5: 240-251. https://doi.org/10.4236/gep.2017.53017

NOMENCLATURE

AB	distance between the current electrodes, m
MN	distance between the measuring electrodes, m
d	density
Rc	Reflection coefficient

Greek symbols

ρ_n	resistivity of the aquifer layer
ρ_{n-1}	resistivity of the layer directly above the aquifer
ρ_s	specific density
ρ_e	density of water
ΔV	measured potential difference